Mon. Not. R. Astron. Soc. **000**, 000–000 (0000) Printed 11 January 2012 (MN LATEX style file v2.2)

On the Evolution of the SFR Function of Massive Galaxies. Constraints at $0.4 < z < 1.8$ from the GOODS-MUSIC Catalogue

Fabio Fontanot[1,2], Stefano Cristiani[1], Paola Santini[3], Adriano Fontana[3], Andrea Grazian[3] and Rachel S. Somerville[4,5]

[1] *INAF-Osservatorio Astronomico, Via Tiepolo 11, I-34131 Trieste, Italy*
[2] *HITS-Heidelberger Institut für Theoretische Studien, Schloss-Wolfsbrunnenweg 35, 69118 Heidelberg, Germany*
[3] *INAF-Osservatorio Astronomico di Roma, via Frascati 33, I-00040, Monteporzio, Italy*
[4] *Space Telescope Science Institute, 3700 San Martin Drive, Baltimore, MD 21218*
[5] *Department of Physics and Astronomy, Johns Hopkins University, Baltimore, MD 21218, USA*
email: fabio.fontanot@h-its.org

arXiv:1112.0029v2 [astro-ph.CO] 10 Jan 2012

Accepted ... Received ...

ABSTRACT

We study the evolution of the Star Formation Rate Function (SFRF) of massive ($M_\star > 10^{10} M_\odot$) galaxies over the $0.4 < z < 1.8$ redshift range and its implications for our understanding of the physical processes responsible for galaxy evolution. We use multiwavelength observations included in the GOODS-MUSIC catalogue, which provides a suitable coverage of the spectral region from 0.3 to 24 μm and either spectroscopic or photometric redshifts for each object. Individual SFRs have been obtained by combining UV and 24 μm observations, when the latter were available. For all other sources an "SED fitting" SFR estimate has been considered. We then define a stellar mass limited sample, complete in the $M_\star > 10^{10} M_\odot$ range and determine the SFRF using the $1/V_{\rm max}$ algorithm. We thus define simulated galaxy catalogues based on the predictions of three different state-of-the-art semi-analytical models of galaxy formation and evolution, and compare them with the observed SFRF. We show that the theoretical SFRFs are well described by a double power law functional form and its redshift evolution is approximated with high accuracy by a pure evolution of the typical SFR (SFR*). We find good agreement between model predictions and the high-SFR end of the SFRF, when the observational errors on the SFR are taken into account. However, the observational SFRF is characterised by a double peaked structure, which is absent in its theoretical counterparts. At $z > 1.0$ the observed SFRF shows a relevant density evolution, which is not reproduced by SAMs, due to the well known overprediction of intermediate mass galaxies at $z \sim 2$. Semi-analytical models are thus able to reproduce the most intense SFR events observed in the GOODS-MUSIC sample and their redshift distribution. At the same time, the agreement at the low-SFR end is poor: all models overpredict the space density of SFR $\sim 1 M_\odot/yr$ and no model reproduces the double peaked shape of the observational SFRF. If confirmed by deeper IR observations, this discrepancy will provide a key constraint on theoretical modelling of star formation and stellar feedback.

Key words: galaxies: evolution - galaxies: fundamental parameters - cosmology: observations

1 INTRODUCTION

The evolution of the star formation rate (SFR) over the cosmic time is a fundamental constraint for every theory of galaxy formation and evolution (see e.g. Hopkins 2004; Hopkins & Beacom 2006). Estimating SFRs for individual galaxies is a complex task, owing to the uncertainties involved in the reconstruction of this quantity from observational data. It is widely accepted that dusty molecular clouds are the main sites for star formation: this implies that newly born stars are subject to significant dust attenuation, until they are able to escape or disrupt their parent

© 0000 RAS

cloud. Young OB stars emit a considerable amount of energy in the restframe ultraviolet (UV) band, which has thus been considered a key waveband for recovering the instantaneous SFR in external galaxies. However, dust absorbs UV photons, heats up and re-emits this energy as thermal radiation in the Infrared (IR) bands. For this reason, SFR estimates based on UV luminosity include correction factors to account for dust attenuation and re-emission (Calzetti et al. 1994; Kennicutt 1998; Bell et al. 2003). Dust attenuation is particularly relevant for star forming galaxies, where the dust emission peak is the dominant component of the galactic spectral energy distribution (SED, see e.g. Calzetti et al. 2000), not to mention the extreme cases of sub-mm galaxies (see e.g. Chapman et al. 2004). The study of the cosmic IR background shows that the global energy emitted by galaxies in the IR is comparable to the direct starlight emission, detectable in the optical (see e.g. Lagache et al. 2005), clearly showing that a significant fraction of star formation activity is expected to be heavily extinguished and detectable only in the IR.

These uncertainties become more relevant, when SFR estimates for galaxies covering a wide redshift range are considered, since both galaxy physical properties and dust properties are expected to evolve with cosmic time (Maiolino et al. 2004; Fontanot et al. 2009a; Gallerani et al. 2010; Fontanot & Somerville 2011). Combining UV information with supplementary information from direct observations in the IR region has thus been proposed as the best tool to account for the total SFR (Kennicutt 1998; Bell et al. 2007). In particular, observations at 24μm have shown to be extremely useful for estimating the global IR luminosity and the instantaneous SFR (Papovich et al. 2007; Santini et al. 2009). Thanks to the advent of the *Herschel* Space Observatory, we will be able to constrain total IR luminosities, by directly sampling the peak of the thermal emission. In fact, it has been recently shown by Rodighiero et al. (2010), that the combination of 24μm data with *Herschel* observations at longer wavelengths represents a very promising tool for a more accurate determination of SFRs of individual galaxies up to $z \sim 3$.

Nowadays, our view of the evolution of galaxy properties has substantially changed thanks to the advent of multiwavelength surveys. If the spectral sampling is fine enough, these catalogues can be used to infer the physical properties also in the absence of spectroscopic information. In recent years several groups (see e.g. Fontana et al. 2004; Panter et al. 2007) developed a number of "SED fitting" algorithms: these codes compare the available photometry for individual sources with synthetic SED libraries and the best-fit model template is chosen by means of a χ^2 minimisation. The resulting estimate for redshift (the so-called photometric redshift), stellar mass ($M_\star$), dust extinction and SFR are the most widely used results of this procedure and have been of fundamental importance for our understanding of galaxy evolution.

The common interpretation of these results is connected to the so-called "downsizing" scenario, in which the star formation shifts from high mass to low mass galaxies as redshift decreases (first introduced by Cowie et al. 1996). This picture has been recently revised by Fontanot et al. (2009b) by showing that the typical errors associated with the estimate of the physical quantities has to be taken into account, when comparing the observed evolutionary trends with the predictions of theoretical models. In particular, Fontanot et al. (2009b) concluded that the discrepancies seen between models and data for massive galaxies are not significant, if model predictions are convolved with typical observational errors, while the strongest discrepancies between model and data are seen for low-to-intermediate mass galaxies.

The importance of the study of the redshift evolution of the cosmic SFR for galaxies at a given mass range has been widely recognised by a number of authors (Noeske et al. 2007; Elbaz et al. 2007; Zheng et al. 2007; Drory & Alvarez 2008; Dunne et al. 2009; Santini et al. 2009; Gilbank et al. 2011). These results and the evolution of the stellar mass density provide fundamental information about the evolution of the global process of galaxy formation. The latter approach is best complemented by the analysis of the stellar mass function (i.e. the volume density of galaxies as a function of stellar mass), which allows us to characterise galaxy evolution as a function of both redshift and stellar mass. Despite the wealth of information already available in the literature about the stellar mass function and its redshift evolution, very little is known about the corresponding Star Formation Rate Function (SFRF hereafter) and its evolution: Bell et al. (2007) studied its evolution in the $0.2 < z < 1.0$ redshift range in the COMBO-17 survey, Schiminovich et al. (2007) presented the distribution of SFRs in the SDSS survey and Bothwell et al. (2011) considered the distribution of SFRs in the Local Volume (defined as an 11 Mpc radius around the Milky Way) combining GALEX and *Spitzer* observations. This is mainly due to the uncertainties involved in the SFR estimate, but also to the difficulties in correctly accounting for the completeness correction needed, especially at the low-SFR end.

In this paper, we focus on a new treatment of the GOODS-MUSIC data, by focusing on a mass complete sample of galaxies. In this way, we are able to fully characterise the various levels of star formation in these objects and follow their redshift evolution. Moreover, since the strongest starbursts are hosted by galaxies above the chosen mass limit, the high-SFR end of the resulting SFRF provides fundamental information about the redshift evolution of this particular galaxy class. Therefore, this paper represents a complementary study of the evolution of SFRs in galaxies of different stellar mass with respect to Santini et al. (2009), to which we refer the reader for the analysis of the evolution of the cosmic SFR and specific SFR. A detailed comparison of the same catalogue with other estimates for the evolution of SFR as a function of redshift and stellar mass has been presented in Fontanot et al. (2009b) (see references herein). In the present paper we focus on the determination of the SFRF and compare results with the predictions of state-of-the-art semi-analytical models of galaxy formation and evolution.

This paper is organised as follows. We present the GOODS-MUSIC catalogue in sec. 2 and the theoretical predictions in sec. 3; we present our results in sec. 4; finally we discuss our conclusions in sec. 5. In the original GOODS-MUSIC papers a Salpeter initial mass function (IMF) is mostly used; throughout this work, we assume a Chabrier IMF and we rescale all stellar mass and SFR estimates, accordingly. We also adopt the ΛCDM concordance cosmological model ($H_0 = 70\,km/s/Mpc$, $\Omega_m = 0.3$ and $\Omega_\lambda = 0.7$).

2 DATASET

Our dataset is based on the updated version of GOOD-MUSIC catalogue (Grazian et al. 2006; Santini et al. 2009). GOODS-MUSIC is a multiwavelength catalogue, with photometry in 15 bands, from 0.35 to 24 μm, covering an area of $\sim 143.2 arcmin^2$ of the GOODS-South field and listing $\sim$ 15000 sources. Main source detection has been performed on the z image, but faint z-band objects detected either on the K image or at 4.5 μm have also been included in the catalogue. The GOODS-MUSIC catalogue has been also cross-correlated with available spectroscopic catalogues, and a spectroscopic redshift has been assigned to $\sim$ 12% of sources. For each source in the catalogue, its physical parameters, such as $M_\star$, SFR and the photometric redshift, have been estimated through a "SED fitting" algorithm (see e.g. Santini et al. 2009 and reference herein); for the purposes of χ^2 minimisation, the available broad band photometry up to rest-frame $\lambda < 5.5\mu$m has been considered. The reference synthetic SED library is defined using Bruzual & Charlot (2003) synthetic models and assuming exponentially declining star formation histories. The relevant parameters for the SED synthesis (such as dust content, metalicity, age, timescale for star formation histories, etc) are defined on a grid in order to cover a wide range of possible values and combinations. The discreteness of SED generation implies that the final estimates for the physical parameters are subject to relevant degeneracies (see e.g. Marchesini et al. 2009 for a discussion focused on the effect of changing the physical ingredients in the adopted stellar population models). In particular, theoretical models predict star formation histories for individual galaxies, which grossly differ from any assumed smooth analytical shape: this has important implications for the $M_\star$ estimate (Stringer et al. 2009). By comparing the available spectroscopic redshifts ($z_{\rm spec}$) with the corresponding estimates from the SED fitting algorithm ($z_{\rm phot}$), Santini et al. (2009) computed the average absolute scatter between spectroscopic and photometric redshift $\Delta z = \frac{|z_{\rm spec} - z_{\rm phot}|}{1+z_{\rm spec}}$. They found $\sigma(\Delta z) = 0.06$ for the whole sample and $\sigma(\Delta z) = 0.043$ when only the brightest galaxies ($z < 23.5$) are considered.

A parallel estimate of the star formation rate is provided by the combination of IR and UV luminosities. For sources in the GOODS-MUSIC sample, Santini et al. (2009) combined the rest-frame UV luminosity derived from the SED fitting and the integrated luminosity between 8 and 1000 micron, obtained by fitting 24 micron fluxes with Dale & Helou (2002) templates. The correction provided by Papovich et al. (2007) has been applied on the resulting SFRs in order to account for the overestimation of the total IR luminosity at high redshifts/IR luminosities when extrapolating from 24 μm fluxes (e.g. Elbaz et al. 2010). Santini et al. (2009) explicitly compared these SFR estimates with the SED fitting results, for sources with both estimates available. They found an overall good agreement, but also a systematic trend at all redshift, with IR-based estimates exceeding the fit-based ones as the star formation rate increases, and vice versa for low values of SFR (see also Papovich et al. 2007; Nordon et al. 2010). In the following of this paper, unless explicitly stated, for each object in the sample we consider IR-based SFRs when available, and "SED fitting" estimates elsewhere.

In order to provide a reliable estimate of statistical quantities like the stellar mass function and the SFR function, a careful analysis of observational biases and selection effects is of fundamental importance for a complete census of all galaxies. Those corrections are critical for the SFRF, given the complex combination of multiwavelength information needed, including both the selection of galaxies in the K-band, fundamental for the definition of a mass-limited sample, and the SFR estimate from 24μm for direct detection (if available) or UV and optical data for the SED fitting procedure. In order to reduce the uncertainties involved in our analysis, we decide to focus on a subsample of the GOOD-MUSIC catalogue, defined by considering only sources with a stellar mass estimate $M_\star > 10^{10} M_\odot$. The GOODS-MUSIC catalogue is expected to be highly complete in this mass range over the whole $0.4 < z < 1.8$ redshift interval, corresponding to K-band magnitudes brighter than $\sim$23 (Fontana et al. 2006). Moreover, for these objects, either 24μm fluxes or detailed multiwavelength photometry are available, and provide reliable estimates for SFR$> 0.01 M_\odot/yr$ (Santini et al. 2009). Objects with documented AGN activity (i.e. spectroscopically determined or X-ray sources) have been removed from the final sample. Compton thick candidates, selected on the basis of their very red spectra (Fiore et al. 2008), have been removed as well. In the redshift range of our interest there are only 4 removed objects with $1.4 < z < 1.8$ (0.5% of the considered sample). We test that our conclusions are robust against the inclusion of these objects. Our final sample consists of 740 sources.

It is also worth mentioning the known overdensities at $z \sim 0.7$ and $z \sim 1.6$ in the GOODS fields, as well as the known underdensity at $z \sim 0.9$ (Gilli et al. 2003; Castellano et al. 2007; Salimbeni et al. 2009). Ongoing surveys like COSMOS (Scoville et al. 2007) and CANDELS (Grogin et al. 2011; Koekemoer et al. 2011), will be able to reduce the effect of cosmic variance on the SFRF determination, and study its environmental dependencies.

3 MODELS

In order to understand the physical implications of our results, we consider the prediction of the recent implementations of 3 state-of-the-art semi-analytical models, namely, the Wang et al. (2008) model, the Somerville et al. (2008) and MORGANA (Monaco et al. 2007). The predictions of these 3 models have been extensively compared in a number of recent papers (Kimm et al. 2009; Fontanot et al. 2009b, 2011) and we refer the reader to these publications and the original papers for all the details of the galaxy formation and evolution modelling. In these models, the evolution of the baryonic component is followed by means of an approximate description of the physical processes at play (such as gas cooling, star formation, stellar feedback, Black Hole growth and AGN feedback) and of their interplay with gravitational processes (i.e. dynamical friction, tidal stripping and two-body mergers), linked to the assembly of the large-scale structure of the Universe. These "recipes" include a number of parameters which are usually fixed by comparing model predictions with a set of low-redshift observations. Despite their simplified approach, SAMs have turned into a flexible and widely used tool to explore a broad range of spe-

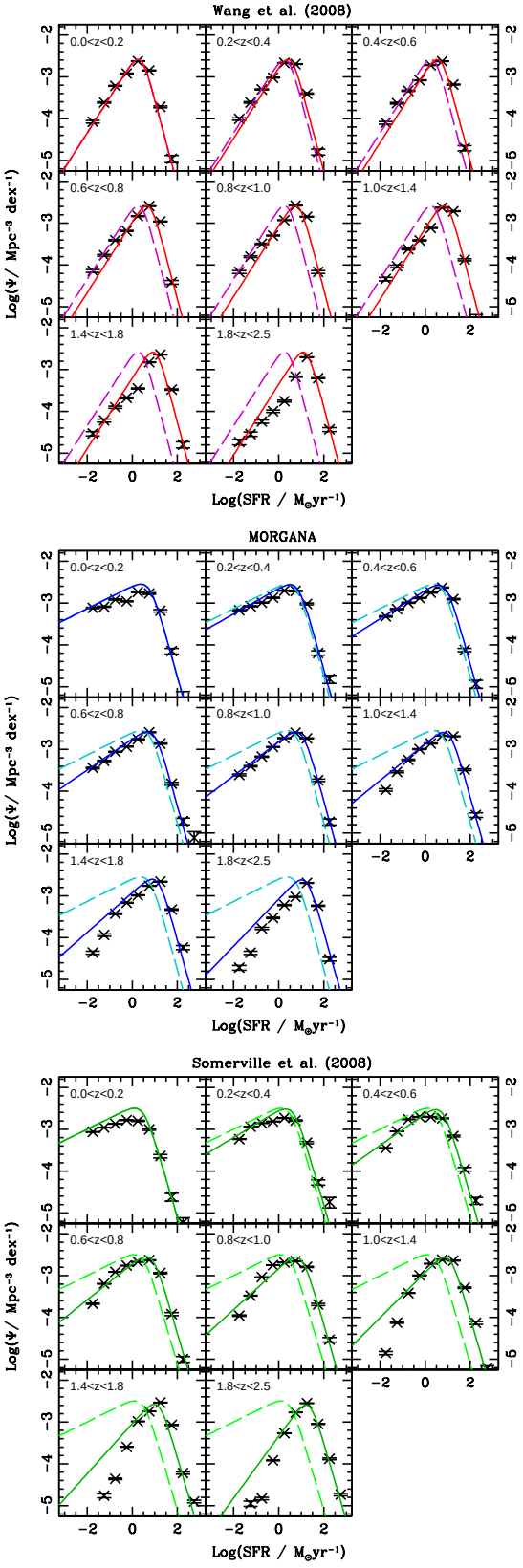


Figure 1. The redshift evolution of the SFRF in semi-analytical models. Crosses refer to the intrinsic predictions of the models, while solid lines show the analytic fit (pure SFR* evolution) of the theoretical SFRF. In each panel, dashed line reports the position of the $z = 0$ SFRF.

cific physical assumptions, as well as the interplay between different physical processes. All models we consider resolve galaxies with $M_\star > 10^9 M_\odot$, and they reproduce fairly well a number of observational constraints on the evolution of the SFR, both as a global quantity (i.e. the cosmic star formation rate), and for individual galactic population (i.e. the fraction of passive galaxies in the local Universe, see e.g. Kimm et al. 2009).

Also for the theoretical predictions, we consider purely stellar mass selected samples ($M_\star > 10^{10} M_\odot$) and, as for the GOOD-MUSIC catalogue, we excluded from the analysis all objects with SFR$< 0.01 M_\odot/yr$. After the selection procedure we are thus left with 385187 galaxies for the Wang et al. (2008) model, 342795 for the Somerville et al. (2008) model and 249823 galaxies for MORGANA. In fig. 1, we show the binned SFRFs for each model (crosses). In order to quantitatively estimate the redshift evolution of the predicted SFRF we apply to model predictions a fitting procedure similar to Fontanot et al. (2007a). We determined best fit analytical solutions to the theoretical predictions assuming both a Schechter and a double power law shape for the SFRF. We use the corresponding number densities to Monte Carlo generate independent data points in the z-SFR space and we calibrate the best fit parameters for the SFRF and its evolution by means of a χ^2 binning procedure. Our results show that the double power law shape systematically scored better results than the Schechter function in terms of χ^2 (with typical values $\chi^2 < 1.0$). This is mainly due to the extra degree of freedom in the high-SFR-end slope, with provides a better description of this region with respect to the exponential cut-off of the Schechter function, even if it is worth stressing that the Schechter shape is not formally ruled out by our analysis. Anyhow, in the following we thus assume a SFRF in the form of a double power-law:

$$\Phi(SFR) = \frac{\Phi^\star(SFR^\star)}{(SFR/SFR^\star)^{-\alpha} + (SFR/SFR^\star)^{-\beta}} \quad (1)$$

where $\Phi^\star$, SFR*, α, β are free parameters. In order to model the redshift evolution of the SFRF we fix the values of the 4 parameters at their $z = 0$ values and we consider different combinations for their redshift evolution. We consider both a pure evolution in SFR* (PSE) of the form:

$$SFR^\star = SFR^\star_{z=0}(1+z)^{k_{\rm SFR}} \quad (2)$$

and a pure density evolution (PDE) of the form:

$$\Phi^\star = \Phi^\star_{z=0} e^{k_\Phi (1+z)} \quad (3)$$

where $k_{\rm SFR}$ and k_Φ represents the evolutionary parameters. Our results point out that the redshift evolution of the theoretical SFRF is in general well described by a pure evolution in SFR*. In fig. 1, we show the best fit results for the Wang et al. (2008) model as a solid red line, while the dashed magenta line represents the corresponding $z = 0.1$ best fit SFRF. As for MORGANA and the Somerville et al. (2008) model, the fit at the low-SFR end is improved (by a factor of 2 in terms of χ^2) if the pure SFR* evolution (which is still statistically acceptable) is combined with an evolution of the slope α of the form:

$$\alpha = \alpha_0 + k_\alpha z \quad (4)$$

where $\alpha_0 = \alpha(z = 0)$ and k_α is the evolutionary parameter. We conclude that a double power law is a good represen-

Table 1. Best fit parameters for the evolution of the SFR function as predicted by semi-analytical models.

SAM	$\Phi^\star(\times 10^{-2})$	$SFR^\star$	$k_{\rm SFR}$	α	β	α_0	k_α	χ^2
Wang et al. (2008)	0.47 ± 0.04	0.29 ± 0.14	2.10 ± 0.64	0.84 ± 0.10	-2.03 ± 0.27	—	—	0.32
Somerville et al. (2008)	0.46 ± 0.05	0.39 ± 0.12	1.99 ± 0.72	—	-1.84 ± 0.24	0.29 ± 0.07	0.23 ± 0.11	0.44
MORGANA	0.41 ± 0.03	0.70 ± 0.17	1.23 ± 0.42	—	-1.95 ± 0.22	0.26 ± 0.03	0.15 ± 0.04	0.29

tation of the SFRF as predicted by the theoretical models at $z < 2$ and for SFR$> 0.01 M_\odot/yr$. We present the best fit parameters corresponding to the above equations in tab. 1. It is worth stressing that we obtain very low χ^2 value even if our fits tend to break down at the highest redshift and lowest SFRs. This is due to the high number of object in the model samples, which thus provide a very accurate fit of the knee of the SFRF and its evolution.

In order to compare the theoretical predictions with the results from the GOODS-MUSIC catalogue, we repeat the fitting procedure after convolving the theoretical predictions with an estimate of the systematic error on the SFR determination, to fully account for the typical observational error in the catalogue (Santini et al. 2009). We assume a log-normal error distribution for the SFR with an amplitude of 0.3 dex (see also Fontanot et al. 2009b). We repeat the above analysis and we determine that a pure SFR* evolution of a double power law is still a good description (i.e. consistent χ^2 values) of the overall redshift evolution of the predicted SFRFs. The most noticeable difference in the best fit parameters is the systematic increase of the β parameter by as much as 20%.

4 RESULTS & DISCUSSION

We first compute the binned SFRF for massive galaxies by means of the standard $1/V_{\rm max}$ formalism, and we show the resulting SFRF in fig. 2 as open circles (cyan circles mark the bin with less than 5 sources). In order to take into account the observational uncertainties, we repeat the analysis 10000 times after convolving every individual SFR estimate with the corresponding error on SFR and redshift (see Santini et al. 2009 for more details on the error estimate). Errorbars in fig. 2 refer to the 1-σ variance over these 10000 realisations. We collect our final estimate of the SFRF and associated errors in tab.2. In the fig. 2 we also include the previous estimate for the SFRF at $z > 0$ from the COMBO-17 survey (Bell et al. 2007). It is worth noting that the COMBO-17 results are obtained by considering all galaxies in their sample, with no cut in stellar mass. Our estimates for the SFRF are in good agreement with the Bell et al. (2007) result at the high-SFR end, where we expect the massive galaxies to dominate the space density.

Fig. 2 clearly show that the COMBO-17 data are not deep enough to explore the low-SFR end with the same extent as in the GOOD-MUSIC catalogue, moreover the low-SFR end of the SFRF shows a very peculiar feature, i.e. a double peaked shape. It is really tempting to interpret this feature in terms of the well known bimodality in the colour (SFR)-mass diagram, and/or connect those galaxies with the intermediate sources populating the so-called *green valley*. It is also worth noting that a populations of rela-

Table 2. SFR Function in the GOODS-MUSIC Catalogue.

	$log(SFR)$	$Log(\Phi(SFR))$
$0.4 < z < 0.6$	-1.75 ± 0.25	$-3.23^{+0.25}_{-0.38}$
	-1.25 ± 0.25	$-3.09^{+0.14}_{-0.18}$
	-0.75 ± 0.25	$-3.53^{+0.22}_{-0.31}$
	-0.25 ± 0.25	$-4.14^{+0.29}_{-0.48}$
	$+0.25 \pm 0.25$	$-3.09^{+0.13}_{-0.16}$
	$+0.75 \pm 0.25$	$-2.81^{+0.09}_{-0.10}$
	$+1.25 \pm 0.25$	$-3.14^{+0.13}_{-0.16}$
	$+1.75 \pm 0.25$	$-3.69^{+0.23}_{-0.34}$
$0.6 < z < 0.8$	-1.75 ± 0.25	$-3.64^{+0.23}_{-0.33}$
	-1.25 ± 0.25	$-2.99^{+0.13}_{-0.15}$
	-0.75 ± 0.25	$-3.04^{+0.12}_{-0.15}$
	-0.25 ± 0.25	$-3.39^{+0.17}_{-0.22}$
	$+0.25 \pm 0.25$	$-3.14^{+0.12}_{-0.15}$
	$+0.75 \pm 0.25$	$-2.88^{+0.09}_{-0.10}$
	$+1.25 \pm 0.25$	$-2.77^{+0.07}_{-0.08}$
	$+1.75 \pm 0.25$	$-3.50^{+0.15}_{-0.19}$
$0.8 < z < 1.0$	-1.75 ± 0.25	$-3.99^{+0.27}_{-0.42}$
	-1.25 ± 0.25	$-3.63^{+0.18}_{-0.24}$
	-0.75 ± 0.25	$-3.99^{+0.20}_{-0.28}$
	-0.25 ± 0.25	$-3.99^{+0.25}_{-0.38}$
	$+0.25 \pm 0.25$	$-3.87^{+0.23}_{-0.34}$
	$+0.75 \pm 0.25$	$-3.30^{+0.12}_{-0.14}$
	$+1.25 \pm 0.25$	$-3.07^{+0.10}_{-0.11}$
	$+1.75 \pm 0.25$	$-3.47^{+0.13}_{-0.16}$
$1.0 < z < 1.2$	-1.75 ± 0.25	$-3.99^{+0.21}_{-0.30}$
	-1.25 ± 0.25	$-3.51^{+0.12}_{-0.15}$
	-0.75 ± 0.25	$-3.61^{+0.13}_{-0.16}$
	-0.25 ± 0.25	$-3.81^{+0.14}_{-0.17}$
	$+0.25 \pm 0.25$	$-3.68^{+0.14}_{-0.17}$
	$+0.75 \pm 0.25$	$-3.31^{+0.08}_{-0.10}$
	$+1.25 \pm 0.25$	$-2.99^{+0.05}_{-0.06}$
	$+1.75 \pm 0.25$	$-3.06^{+0.05}_{-0.06}$
	$+2.25 \pm 0.25$	$-4.29^{+0.19}_{-0.25}$
	$+2.75 \pm 0.25$	$-4.59^{+0.29}_{-0.49}$
$1.2 < z < 1.8$	-1.75 ± 0.25	$-4.49^{+0.31}_{-0.54}$
	-1.25 ± 0.25	$-4.37^{+0.22}_{-0.32}$
	-0.75 ± 0.25	$-3.72^{+0.14}_{-0.18}$
	-0.25 ± 0.25	$-3.83^{+0.17}_{-0.21}$
	$+0.25 \pm 0.25$	$-4.13^{+0.16}_{-0.21}$
	$+0.75 \pm 0.25$	$-3.80^{+0.14}_{-0.18}$
	$+1.25 \pm 0.25$	$-3.47^{+0.09}_{-0.10}$
	$+1.75 \pm 0.25$	$-3.40^{+0.07}_{-0.07}$
	$+2.25 \pm 0.25$	$-3.45^{+0.07}_{-0.08}$
	$+2.75 \pm 0.25$	$-4.37^{+0.22}_{-0.31}$

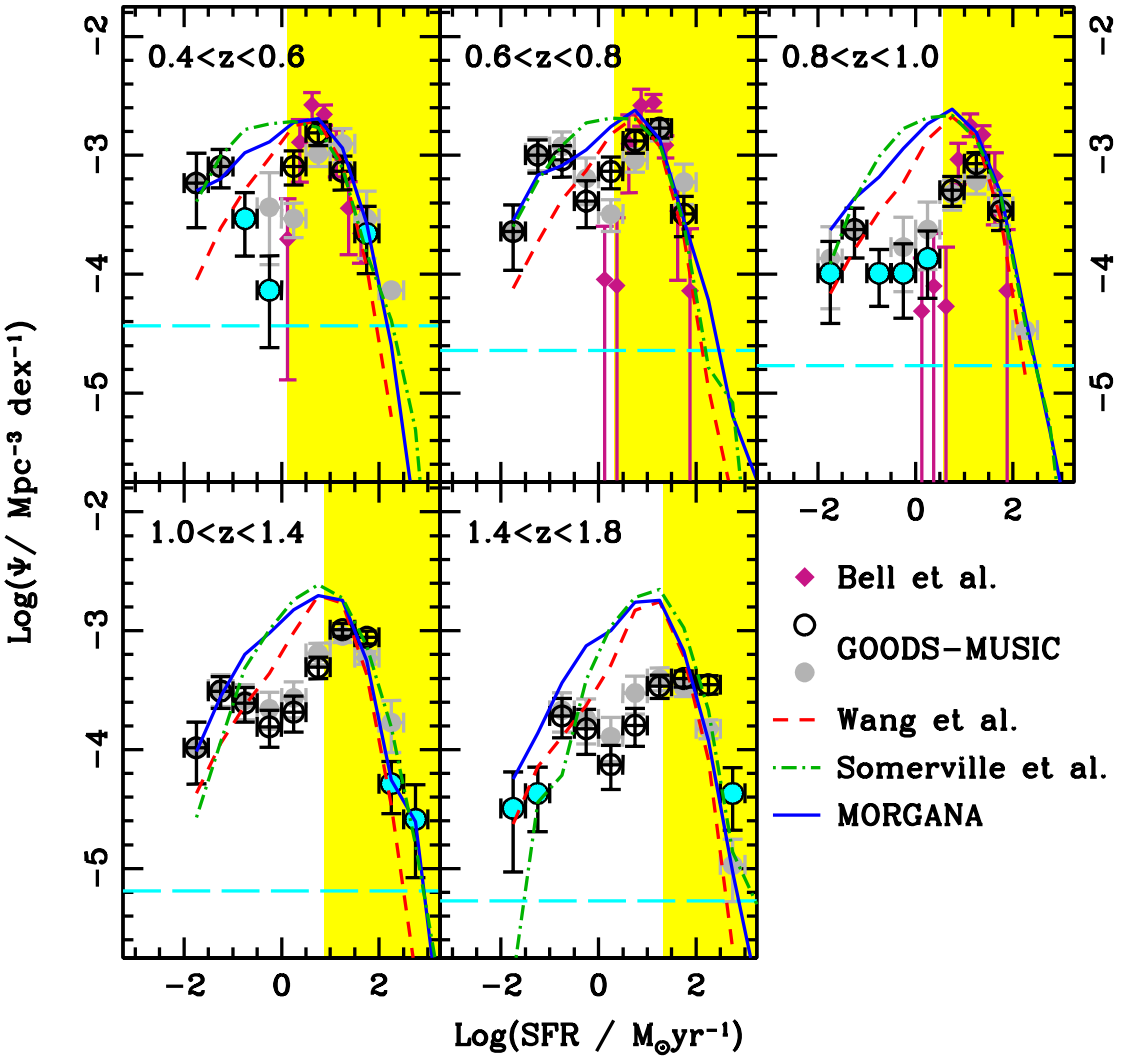


Figure 2. The evolution of the SFRF for $M > 10^{10} M_{\odot}$ galaxies in the GOOD-MUSIC sample. In each panel, the horizontal cyan long-dashed line represents the space density corresponding to one object in the GOODS-MUSIC volume, while the yellow shading highlights the the SFR range covered by 24μm observations in each redshift bin. Open circles refer to our SFRF estimate from the GOODS-MUSIC survey: in each subpanel, cyan solid circles mark the bins with less than 5 galaxies; errorbars represent the 1-σ confidence levels (see text for more details). Light grey filled circles refer to the SFRF derived only from the results of the SED fitting algorithm. Purple diamonds refer to the SFRF estimate from the COMBO-17 (Bell et al. 2007) survey. In all panels, dashed red, dot-dashed green and solid blue lines refer to the Wang et al. (2008), Somerville et al. (2008) and MORGANA predictions, respectively. SAM predictions are convolved with an Gaussian error on the SFR (width 0.3 dex, see text).

tively massive galaxies with very low levels of star formation has been already reported at lower redshifts (Wilman et al. 2008; Schawinski et al. 2010).

However, a word of caution is necessary. We have limited information about individual 24μm fluxes for galaxies in our mass-selected sample, and typically only for SFR$> 1 M_{\odot}/yr$. This implies that the secondary peak at SFR$< 1 M_{\odot}/yr$ is populated by galaxies whose SFR estimate comes from the SED fitting algorithm. In order to test the robustness of our result, we repeat our analysis considering only SFR estimates coming from the SED fitting. We find no significant change in the shape of the resulting SFRF (light grey filled circles in fig. 2): in particular, the double peaked behaviour persists. Our main conclusions are therefore insensitive to the origin of SFR estimate, in agreement with Santini et al. (2009) results (i.e. the 24μm-based SFR estimates are in reasonable agreement with SED fitting results for sources with both estimates available).

Nonetheless, we cannot completely exclude the hypothesis that the gap between the two peaks is an artifact of the SED fitting procedure (i.e. piling up of low-SFR galaxies in the secondary peak, due to the coarse grid-sampled properties of the synthetic SED library). We plan to study the efficiency of the SED fitting algorithm in the estimate of SFRs in the range $0.1 M_{\odot}/yr <$ SFR $< 10 M_{\odot}/yr$ as a part of a larger programme, comparing the global performances of

our algorithm in recovering the physical properties of model galaxies with complex star formation histories, starting from synthetic photometry extracted from SAM simulated catalogues. A similar procedure has been recently employed by Lee et al. (2009) to a sample of high-redshift model galaxies: they found that SED fitting underestimates SFR in their sample and attributed this behaviour to to the different star formation histories predicted by SAMs with respect to those assumed in the reference synthetic SED libraries.

As a preliminary test we consider a small sample of 5000 model galaxies with $0.4 < z < 1.8$ taken from the same MORGANA realisation and uniformly distributed in SFR. For the purpose of this test we do not limit the sample to $M_\star > 10^{10} M_\odot$ model galaxies. For each object, we compute a synthetic SED using the Radiative-Transfer code GRASIL (Silva et al. 1998, see also Fontanot et al. 2007b). We then apply the SED fitting algorithm to the corresponding synthetic photometry. In fig. 3 (upper panel) we compare the original, flat, distribution of SFR in our sample (black histogram) with the distribution of reconstructed SFRs (blue shaded histograms). This test suggests that some depletion effects in SFR distribution may be effective at SFR below our fiducial limit (SFR $\sim 0.01 M_\odot/yr$); however, the SFR distribution in the region corresponding to the secondary peak and the valley (roughly identified by the green arrows) does not seem to be affected by any obvious systematic effect. We also repeat the same analysis on a subsample of $M_\star > 10^{10} M_\odot$ model galaxies, (lower panel), whose distribution is more similar to the theoretical SFRF. Again we obtain no obvious systematic effect in SED fitting reconstruction. We also check that similar results hold if we split the sample in smaller redshift bins, but with less statistical significance, due to the reduced dimensions of the subsamples.

In fig. 2 we also show the predictions of our three SAMs as coloured lines: the level of agreement between the 3 models is striking, given the very different star formation and stellar feedback schemes adopted. In particular we stress that the predicted redshift evolution of the typical SFR* is remarkably similar between all models. This is due to the external constraints (i.e. the evolution of the cosmic SFR) used to calibrate the models. The strongest discrepancies are seen at the low-SFR end of the SFRF and clearly show the importance of using constraints based on the SFRF, in order to disentangle between different theoretical approaches to star formation and stellar feedback.

The comparison between theoretical predictions and the observational results from the GOODS-MUSIC survey shows a remarkably good agreement at the high-SFR end, where the available 24μm observations are deep enough to constrain its shape and evolution out to $z \sim 1.8$ (yellow shaded region in fig. 2). Therefore we conclude that SAMs provide a satisfactory description for the space density of galaxies with SFR$> 10 M_\odot/yr$ at moderate redshifts. It worth stressing that accounting for observational errors is essential for the correct interpretation of the comparison between model and data: the error-free intrinsic SFRFs would underpredict the space density of the strongest starbursts by a factor of a few.

Observations at 24μm are also able to constrain the position of the peak of the SFRF out to $z \sim 1$ (and give some indications for its position at higher redshifts). In order to get more insight on the evolution of the typical SFR of galaxies at different redshifts, we repeat on the data the same fitting procedure described in sec. 3. Given the double peaked shape of the observed SFRF both a double power law and a Schechter function are no longer a good representation of the SFRF over the whole SFR range. Therefore, we chose to repeat the fitting procedure both on the reference sample ($SFR > 0.01 M_\odot/yr$), and on a smaller sample containing only sources with $SFR > 1 M_\odot/yr$ (i.e. focusing on the primary SFRF peak). This choice has no major impact on our conclusions; as expected only the low-SFR-end slope α show a relevant variation between the two samples. We collect our final results in tab. 3. The results show that the SFRF, as depicted by the GOODS-MUSIC survey, shows a remarkable density evolution (PDE) in the $0.8 < z < 1.8$ range, and a milder SFR* evolution (PSE) over the whole redshift range. The theoretical SFRF is able to reproduce the SFR* evolution, although it peaks systematically at lower typical SFR than the observational constraints, but its density evolution is negligible. This represents a first relevant discrepancy between models and data and it is due to the well documented overprediction of the space density of $10^{10} M_\odot < M_\star < 10^{11} M_\odot$ galaxies at $1.0 < z < 1.8$ seen in the models and in the data; Fontanot et al. (2009b) showed that SAMs predict for these galaxies space densities very similar to the local value out to $z \sim 1.8$, while their observed stellar mass function show a remarkable evolution (their fig.1). This implies that the negligible density evolution predicted for the SFRF at $z > 1.0$ is related to the too efficient formation of intermediate mass galaxies in SAMs (see also Lo Faro et al. 2009).

The most interesting discrepancies between models and

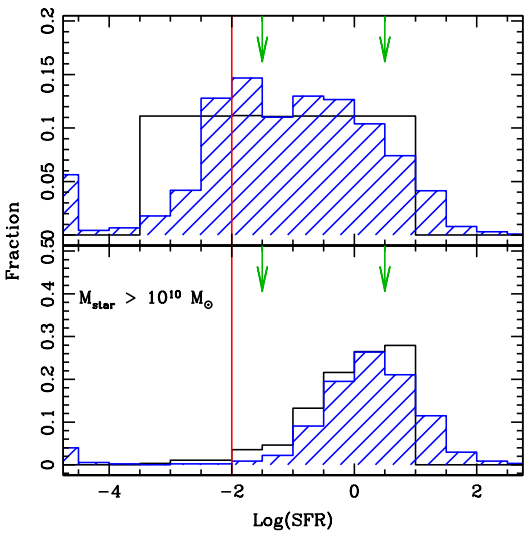


Figure 3. Test on the SED fitting algorithm. *Upper panel*: comparison of the SFR distribution in a sample of $0.4 < z < 1.8$ MORGANA model galaxies (solid black histogram), with the corresponding distribution of reconstructed SFRs, obtained applying the SED fitting algorithm to synthetic photometry (blue hatched histogram). Red line represents the limiting SFR considered in the Santini et al. (2009) paper, while green arrow bracket the region containing the main features of the observed SFRF. *Lower Panel*: same as upper panel, but for a sample of $M_\star > 10^{10} M_\odot$ model galaxies.

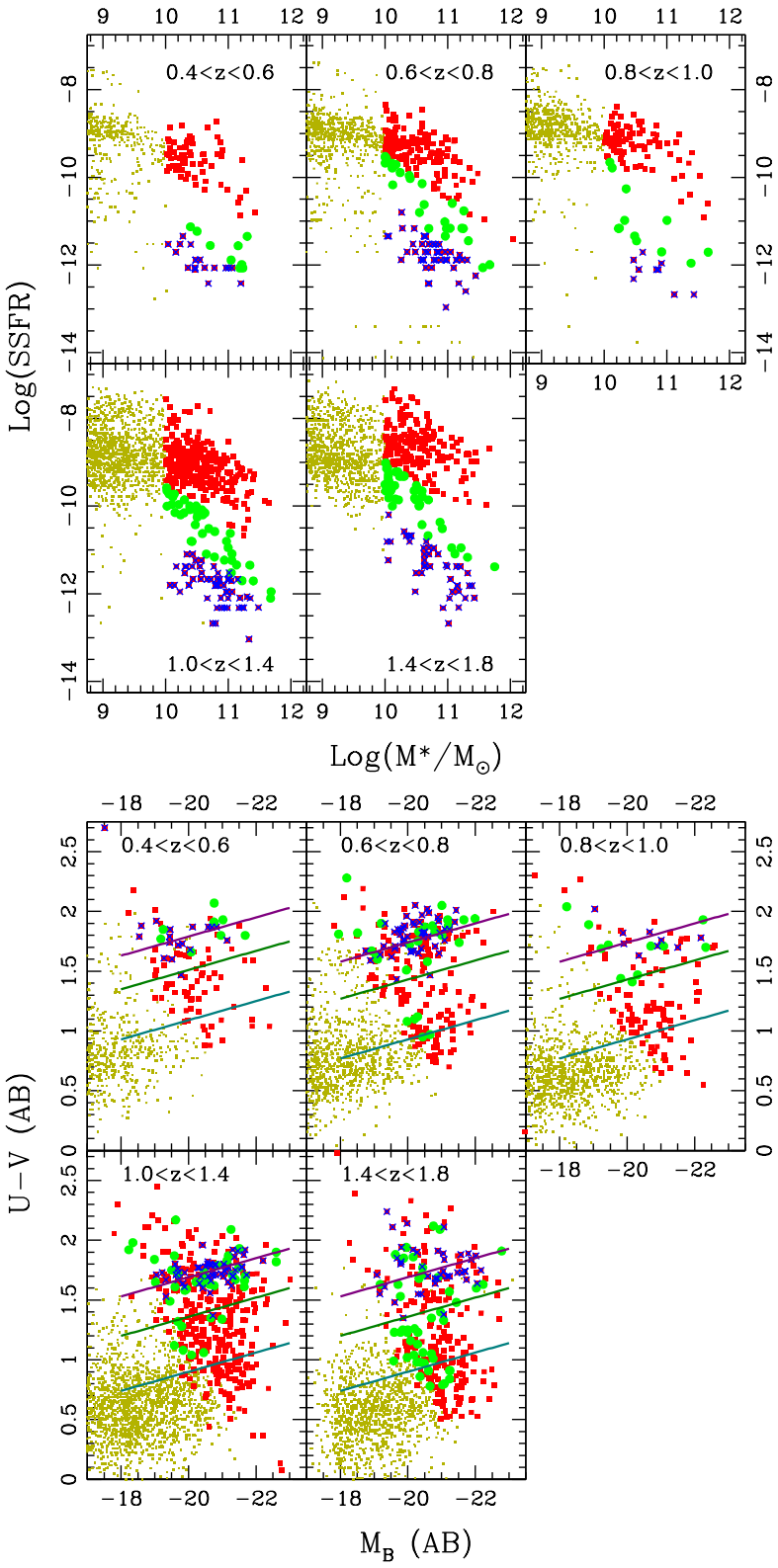


Figure 4. *Upper panel:* Specific SFR versus $M_\star$ *Lower panel:* Rest-Frame colour-magnitude diagrams. In each panel the yellow dots refer to the K-limited GOODS-MUSIC sample; red dots mark sources with $M_\star > 10^{10} M_\odot$ and SFR $> 0.01 M_\odot/yr$; blue crosses refer to galaxies belonging the secondary peak on the SFRF at each redshift bin, while green circles refer to galaxies with SFR intermediate between the two peaks. In the lower panel, dark red and blue lines refer to the mean $U-V$ colours along the red sequence and the blue cloud, while the dark green solid line reproduces the divider between the blue and red populations (see Salimbeni et al. 2008 for more details).

Table 3. Best fit parameters for the evolution of the SFR function in the GOODS-MUSIC Catalogue.

Model	$\Phi^\star(\times 10^{-2})$	$SFR^\star$	$k_{\rm SFR}$	k_Φ	α	β	χ^2
			$Log(SFR) > -2.0$				
PDE	0.37 ± 0.11	1.13 ± 0.13	0.70 ± 0.58	—	unconstr.	-1.77 ± 0.30	2.7
PSE	0.74 ± 0.20	1.30 ± 0.07	—	-1.09 ± 0.60	unconstr.	-1.85 ± 0.29	1.6
PDE+PSE	0.88 ± 0.16	0.81 ± 0.11	2.07 ± 0.44	-1.22 ± 0.22	unconstr.	-1.43 ± 0.31	1.2
			$Log(SFR) > 0.0$				
PDE	0.30 ± 0.05	1.02 ± 0.19	0.93 ± 0.35	—	unconstr.	-1.84 ± 0.21	1.5
PSE	0.58 ± 0.16	1.31 ± 0.11	—	-0.72 ± 0.23	unconstr.	-1.48 ± 0.24	0.9
PDE+PSE	0.55 ± 0.05	0.54 ± 0.15	2.09 ± 0.38	-0.56 ± 0.11	unconstr.	-1.43 ± 0.24	0.6

data are indeed seen at the low-SFR end: all SAMs predict a featureless low-SFR end, whose slope (and its redshift evolution) depends on the details of the treatment of SFR and stellar feedback. The most relevant difference between data and model prediction is the fact that all models overpredict the abundance of SFR$\sim 1 M_\odot/yr$ sources. It is also interesting to notice that no model reproduces the double peaked feature of the observed SFRF.

There are at least two possible interpretations of our results. First (scenario A), as it has been suggested by many authors (see e.g., De Lucia & Blaizot 2007; Wang et al. 2007), SAMs predict too low SFRs for most of the galaxies in the mass range of our interest: they have SFRs well below the detection limit of our sample, and, overall, they are too passive at intermediate redshifts (Fontanot et al. 2009b). The three models indeed predict a secondary peak in their SFR distribution, and it consists of completely passive galaxies (SFR= 0, see e.g. figure 4 in Fontanot et al. 2009b). In this scenario, we could interpret the observed secondary peak (at low, but still detectable SFRs), if confirmed by deeper observations, as an evidence that models are not able to reproduce the correct space density for galaxies migrating from the blue cloud to the red sequence (see also Cassata et al. 2007), and we could interpret it as an indication that galaxies in the GOODS-MUSIC sample move in the colour-magnitude diagram at a slower pace with respect to theoretical expectations. This scenario is also consistent with the recent findings of Lagos et al. (2011): they revisited the definition of the star formation law in the context of the GALFORM SAM (Baugh et al. 2005; Bower et al. 2006) taking into account recent results on the relation between star formation and the atomic and molecular gas content of galaxies (see e.g. Blitz & Rosolowsky 2006; Krumholz et al. 2009). They showed that the properties of galaxies with low SFRs (and their redshift evolution on the $M_\star$ versus SFR plane) are particularly sensitive to the details of the assumed star formation law, and suitable modifications to the standard prescriptions may indeed lead to bimodal SFR distributions in the direction needed to explain our results.

An alternative scenario (scenario B) requires small SFR retriggering events in already red galaxies (see e.g. Treu et al. 2005): these events might be linked to the dynamical evolution of galaxies in dense environments (mergers, interactions). Therefore this also implies a dependence of these secondary SFR events on the environment, which in principle could be accessible by larger surveys (see e.g. Cucciati et al. 2010 and references herein). Another possible origin for small and late star formation episodes in massive galaxies might be related to the duty cycles associated to the "radio-mode" AGN activity (Fontanot et al. 2011): if the injection of energy from the central Black Hole into the surrounding Dark Matter halo is not a continuous event, some cold gas might still be allowed to infall onto massive galaxies.

In order to get more insight in the properties of galaxies responsible for this feature, we consider the distribution of the GOODS-MUSIC galaxies both in the specific SFR versus $M_\star$ and in rest-frame colour-magnitude diagram (as reconstructed from the SED fitting algorithm) in fig 4. In both panels, we mark the $M_\star > 10^{10} M_\odot$ galaxies as red squares; blue crosses and green circles refer to the galaxies belonging to the secondary peak and lying between the two peaks respectively. Dark red, green and blue lines in the lower panel reproduce the locus of red sequence, green valley and blue cloud as defined in Salimbeni et al. (2008).

We expect the two scenarios we discuss in the previous paragraph to predict a different colour evolution for galaxies. In scenario A, we assume a continuity between the colour of galaxies belonging to the primary peak, valley and secondary peak, in terms of blue cloud, "green valley" and red sequence. Since scenario A assumes a continuous motion of galaxies from the blue cloud to the red sequence, we expect galaxies with different SFRs to populate well defined regions of the colour-magnitude diagram. The relative abundance of galaxies in the different regions of the diagram is an indication of the time they spend in the different phases.

On the other hand, in scenario B we expect a larger spread of galaxies belonging to the secondary peak in the colour magnitude diagram. The physical processes responsible for the retriggering have a strong dependence on the stellar mass and/or environment of galaxies, and are almost insensitive to the position of the galaxy in the colour-magnitude diagram at the time of the retriggering. Therefore, the relative tightness of the locus where secondary peak objects are found in the rest-frame colour-magnitude diagrams is in qualitative agreement with the former scenario. On the other hand, galaxies with SFR intermediate between the two peaks show a much wider distribution in fig. 4. We warn the reader that these are qualitative conclusions that rely on the assumption that the $U-V$ colour is a fair tracer of the SFR activity, and that this colour is also sensitive enough to the low-levels of SFR for galaxies in the secondary peak. The fact that most of SFR estimates for sources below the SFRF peak have been derived from SED fitting also pre-

vents firm conclusions on this issue from GOODS-MUSIC data alone. A more quantitative analysis will require better estimates for SFR levels in galaxy population and better tracers of physical state of galaxies belonging to the different regions of the colour-magnitude diagram, and it is beyond the aims of the present work.

5 CONCLUSIONS

In this paper we consider the GOODS-MUSIC sample to study the SFR function and its redshift evolution in the redshift range $0.4 < z < 1.8$, just after the peak in the cosmic SFR, a fundamental epoch to understand the physical processes responsible for the decline of star forming activity as a function of galaxy stellar mass. In order to reduce the effect of completeness corrections, we restrict our analysis to galaxies with $M_\star > 10^{10} M_\odot$, since at these stellar masses the GOODS-MUSIC is expected to be a complete sample. We thus compute the SFRF using SFR estimates coming from both SED fitting and/or a combination of UV light with 24μm observations. We compare the resulting SFRF with the predictions of 3 independent semi-analytical models of galaxy formation and evolution (Wang et al. 2008; Somerville et al. 2008 and MORGANA) and we obtain the following results:

- The agreement between the observed and predicted high-SFR end (SFR$> 10 M_\odot/yr$) of the SFRF is good over the whole redshift range (once the observational errors are taken into account). This result implies that theoretical models are able to reproduce the space density evolution of the strongest starbursts. It is worth noting that the predictions of the three models are remarkably similar in this SFR range.
- The SFRF of massive galaxies, as seen by the GOODS-MUSIC is characterised by a complex evolution both in the typical SFR and in the normalisation. Theoretical models are able to cope with the SFR* evolution, but they predict a negligible density evolution. In particular, all models overpredict the space density of SFR $\sim 1 M_\odot/yr$ galaxies. We interpret this behaviour as due to the well documented excess of intermediate mass galaxies ($10^{10} M_\odot < M_\star < 10^{11} M_\odot$) in SAMs (Fontanot et al. 2009b).
- The observed low-SFR end of SFRF is characterised by a double peaked shape. Despite the uncertainties in the determination of such low SFRs from SED fitting methods, it is worth noting that none of the theoretical model we consider is able to reproduce this feature, and all of them predict a smooth decrease of the space density of low-SFR galaxies, with a well defined power-law slope α. Since this is also the SFR range where models differ most, each of them predicting a different value for α, we stress that future observations providing stronger constraints on the low-SFR end of the SFRF will be of fundamental importance to understand the physical mechanisms responsible for the decline of SFR since $z \sim 2$ in massive galaxies.

The main result of this paper lies in the analysis at the high-SFR end, since this region is completely sampled by 24μm observations, which are critical for the recovery of the SFR levels. Also the evolution of the typical SFR* is well sampled by means of IR data out to $z \sim 1.0$, and allow us to put strong constraint on this relevant discrepancy seen between data and models. Unfortunately, for lower SFR levels this information is not currently available, and we have to rely entirely on the results of SED fitting. Our tests suggest that the use of SED fitting results does not introduce any obvious distortion in the SFR distribution at intermediate SFR values, but we could not completely exclude the double peaked feature in the SFRF to be due to systematics in the SED fitting algorithm. From optical photometry alone is not possible to uniquely associate SFR $\sim 1 M_\odot/yr$ galaxies (the region were models and data differ most and roughly corresponding to the region between the two peaks of the SFRF) with known populations in the colour-magnitude diagram, i.e. the green valley or the blue cloud. The red $U-V$ colours, with a relatively small scatter, of galaxies belonging to the putative secondary peak provide only a qualitative support to a scenario where star formation in massive galaxies decrease at a slower pace with respect to theoretical expectations. If confirmed, this double peaked shape of the SFRF would thus represent a critical discrepancy between models and observations, since all SAMs we consider predict a smooth, featureless, single slope power-law shape for the SFRF. Modifications in the assumed star formation law, taking into account the relation between star formation and the atomic and molecular gas content of galaxies may alleviate this tension, since the properties of model galaxies with low SFR levels are very sensitive to this modeling layer (Lagos et al. 2011, see e.g.).

On the other hand, thanks to the new facilities (e.g. *Herschel*), future observations in the IR region, able to characterise the properties of the IR peak, will finally determine the SFR levels of these objects and the relevance of this feature. This is a fundamental task, since the low-SFR end of the SFRF is the region where SAM predictions differ most and therefore provides potentially strong constraints to the different approaches to star formation and stellar feedback.

ACKNOWLEDGEMENTS

We thank Gabriella De Lucia and Pierluigi Monaco for stimulating discussions. We are grateful to Jie Wang for letting us use the outputs of his simulations. FF acknowledges the support of an INAF-OATs fellowship granted on 'Basic Research' funds and financial contribution from the ASI project "IR spectroscopy of the Highest Redshift BH candidates" (agreement ASI-INAF 1/009/10/00).

REFERENCES

Baugh C. M., Lacey C. G., Frenk C. S., Granato G. L., Silva L., Bressan A., Benson A. J., Cole S., 2005, MNRAS, 356, 1191
Bell E. F., McIntosh D. H., Katz N., Weinberg M. D., 2003, ApJS, 149, 289
Bell E. F., Zheng X. Z., Papovich C., Borch A., Wolf C., Meisenheimer K., 2007, ApJ, 663, 834
Blitz L., Rosolowsky E., 2006, ApJ, 650, 933
Bothwell M. S., Kenicutt R. C., Johnson B. D., Wu Y., Lee J. C., Dale D., Engelbracht C., Calzetti D., Skillman E., 2011, MNRAS, 415, 1815

Bower R. G., Benson A. J., Malbon R., Helly J. C., Frenk C. S., Baugh C. M., Cole S., Lacey C. G., 2006, MNRAS, 370, 645
Bruzual G., Charlot S., 2003, MNRAS, 344, 1000
Calzetti D., Armus L., Bohlin R. C., Kinney A. L., Koornneef J., Storchi-Bergmann T., 2000, ApJ, 533, 682
Calzetti D., Kinney A. L., Storchi-Bergmann T., 1994, ApJ, 429, 582
Cassata P., Guzzo L., Franceschini A., Scoville N., Capak P., Ellis R. S., Koekemoer A., McCracken H. J., Mobasher B., Renzini A., Ricciardelli E., Scodeggio M., Taniguchi Y., Thompson D., 2007, ApJS, 172, 270
Castellano M., Salimbeni S., Trevese D., Grazian A., Pentericci L., Fiore F., Fontana A., Giallongo E., Santini P., Cristiani S., Nonino M., Vanzella E., 2007, ApJ, 671, 1497
Chapman S. C., Smail I., Windhorst R., Muxlow T., Ivison R. J., 2004, ApJ, 611, 732
Cowie L. L., Songaila A., Hu E. M., Cohen J. G., 1996, AJ, 112, 839
Cucciati O., Iovino A., Kovač K., Scodeggio M., Lilly S. J., Bolzonella M., Bardelli S., Vergani D. e. a., 2010, A&A, 524, A2+
Dale D. A., Helou G., 2002, ApJ, 576, 159
De Lucia G., Blaizot J., 2007, MNRAS, 375, 2
Drory N., Alvarez M., 2008, ApJ, 680, 41
Dunne L., Ivison R. J., Maddox S., Cirasuolo M., Mortier A. M., Foucaud S., Ibar E., Almaini O., Simpson C., McLure R., 2009, MNRAS, 394, 3
Elbaz D., Daddi E., Le Borgne D., Dickinson M., Alexander D. M., Chary R.-R., Starck J.-L., Brandt W. N., Kitzbichler M., MacDonald E., Nonino M., Popesso P., Stern D., Vanzella E., 2007, A&A, 468, 33
Elbaz D., Hwang H. S., Magnelli B., Daddi E., Aussel H., Altieri B., Amblard A., Andreani P. e. a., 2010, A&A, 518, L29+
Fiore F., Grazian A., Santini P., Puccetti S., Brusa M., Feruglio C., Fontana A., Giallongo E., Comastri A., Gruppioni C., Pozzi F., Zamorani G., Vignali C., 2008, ApJ, 672, 94
Fontana A., Pozzetti L., Donnarumma I., Renzini A., Cimatti A., Zamorani G., Menci N., Daddi E., Giallongo E., Mignoli M., Perna C., Salimbeni S., Saracco P., Broadhurst T., Cristiani S., D'Odorico S., Gilmozzi R., 2004, A&A, 424, 23
Fontana A., Salimbeni S., Grazian A., Giallongo E., Pentericci L., Nonino M., Fontanot F., Menci N., Monaco P., Cristiani S., Vanzella E., de Santis C., Gallozzi S., 2006, A&A, 459, 745
Fontanot F., Cristiani S., Monaco P., Nonino M., Vanzella E., Brandt W. N., Grazian A., Mao J., 2007a, A&A, 461, 39
Fontanot F., De Lucia G., Monaco P., Somerville R. S., Santini P., 2009b, MNRAS, 397, 1776
Fontanot F., Monaco P., Silva L., Grazian A., 2007b, MNRAS, 382, 903
Fontanot F., Pasquali A., De Lucia G., van den Bosch F. C., Somerville R. S., Kang X., 2011, MNRAS, 413, 957
Fontanot F., Somerville R. S., 2011, MNRAS, 416, 2962
Fontanot F., Somerville R. S., Silva L., Monaco P., Skibba R., 2009a, MNRAS, 392, 553
Gallerani S., Maiolino R., Juarez Y., Nagao T., Marconi A., Bianchi S., Schneider R., Mannucci F., Oliva T., Willott C. J., Jiang L., Fan X., 2010, A&A, 523, A85+
Gilbank D. G., Bower R. G., Glazebrook K., Balogh M. L., Baldry I. K., Davies G. T., Hau G. K. T., Li I. H., McCarthy P., Sawicki M., 2011, MNRAS, 414, 304
Gilli R., Cimatti A., Daddi E., Hasinger G., Rosati P., Szokoly G., Tozzi P., Bergeron J., Borgani S., Giacconi R., Kewley L., Mainieri V., Mignoli M., Nonino M., Norman C., Wang J., Zamorani G., Zheng W., Zirm A., 2003, ApJ, 592, 721
Grazian A., Fontana A., de Santis C., Nonino M., Salimbeni S., Giallongo E., Cristiani S., Gallozzi S., Vanzella E., 2006, A&A, 449, 951
Grogin N. A., Kocevski D. D., Faber S. M., Ferguson H. C., Koekemoer A. M., Riess A. G., Acquaviva V., Alexander D. M. e. a., 2011, ApJS, 197, 35
Hopkins A. M., 2004, ApJ, 615, 209
Hopkins A. M., Beacom J. F., 2006, ApJ, 651, 142
Kennicutt Jr. R. C., 1998, ApJ, 498, 541
Kimm T., Somerville R. S., Yi S. K., van den Bosch F. C., Salim S., Fontanot F., Monaco P., Mo H., Pasquali A., Rich R. M., Yang X., 2009, MNRAS, 394, 1131
Koekemoer A. M., Faber S. M., Ferguson H. C., Grogin N. A., Kocevski D. D., Koo D. C., Lai K., Lotz J. M. e. a., 2011, ApJS, 197, 36
Krumholz M. R., McKee C. F., Tumlinson J., 2009, ApJ, 699, 850
Lagache G., Puget J.-L., Dole H., 2005, ARA&A, 43, 727
Lagos C. D. P., Lacey C. G., Baugh C. M., Bower R. G., Benson A. J., 2011, MNRAS, 416, 1566
Lee S.-K., Idzi R., Ferguson H. C., Somerville R. S., Wiklind T., Giavalisco M., 2009, ApJS, 184, 100
Lo Faro B., Monaco P., Vanzella E., Fontanot F., Silva L., Cristiani S., 2009, MNRAS, 399, 827
Maiolino R., Schneider R., Oliva E., Bianchi S., Ferrara A., Mannucci F., Pedani M., Roca Sogorb M., 2004, Nature, 431, 533
Marchesini D., van Dokkum P. G., Förster Schreiber N. M., Franx M., Labbé I., Wuyts S., 2009, ApJ, 701, 1765
Monaco P., Fontanot F., Taffoni G., 2007, MNRAS, 375, 1189
Noeske K. G., Faber S. M., Weiner B. J., Koo D. C., Primack J. R., Dekel A., Papovich C., Conselice C. J., Le Floc'h E., Rieke G. H., Coil A. L., Lotz J. M., Somerville R. S., Bundy K., 2007, ApJ, 660, L47
Nordon R., Lutz D., Shao L., Magnelli B., Berta S., Altieri B., Andreani P., Aussel H. e. a., 2010, A&A, 518, L24+
Panter B., Jimenez R., Heavens A. F., Charlot S., 2007, MNRAS, 378, 1550
Papovich C., Rudnick G., Le Floc'h E., van Dokkum P. G., Rieke G. H., Taylor E. N., Armus L., Gawiser E., Huang J., Marcillac D., Franx M., 2007, ApJ, 668, 45
Rodighiero G., Cimatti A., Gruppioni C., Popesso P., Andreani P., Altieri B., Aussel H., Berta S. e. a., 2010, A&A, 518, L25+
Salimbeni S., Castellano M., Pentericci L., Trevese D., Fiore F., Grazian A., Fontana A., Giallongo E., Boutsia K., Cristiani S., de Santis C., Gallozzi S., Menci N., Nonino M., Paris D., Santini P., Vanzella E., 2009, A&A, 501, 865
Salimbeni S., Giallongo E., Menci N., Castellano M., Fontana A., Grazian A., Pentericci L., Trevese D., Cristiani S., Nonino M., Vanzella E., 2008, A&A, 477, 763

Santini P., Fontana A., Grazian A., Salimbeni S., Fiore F., Fontanot F., Boutsia K., Castellano M., Cristiani S., de Santis C., Gallozzi S., Giallongo E., Menci N., Nonino M., Paris D., Pentericci L., Vanzella E., 2009, A&A, 504, 751
Schawinski K., Urry C. M., Virani S., Coppi P., Bamford S. P., Treister E., Lintott C. J., Sarzi M. e. a., 2010, ApJ, 711, 284
Schiminovich D., Wyder T. K., Martin D. C., Johnson B. D., Salim S., Seibert M., Treyer M. A., Budavári T. e. a., 2007, ApJS, 173, 315
Scoville N., Aussel H., Brusa M., Capak P., Carollo C. M., Elvis M., Giavalisco M., Guzzo L. e. a., 2007, ApJS, 172, 1
Silva L., Granato G. L., Bressan A., Danese L., 1998, ApJ, 509, 103
Somerville R. S., Hopkins P. F., Cox T. J., Robertson B. E., Hernquist L., 2008, MNRAS, 391, 481
Stringer M. J., Benson A. J., Bundy K., Ellis R. S., Quetin E. L., 2009, MNRAS, 393, 1127
Treu T., Ellis R. S., Liao T. X., van Dokkum P. G., Tozzi P., Coil A., Newman J., Cooper M. C., Davis M., 2005, ApJ, 633, 174
Wang J., De Lucia G., Kitzbichler M. G., White S. D. M., 2008, MNRAS, 384, 1301
Wang L., Li C., Kauffmann G., De Lucia G., 2007, MNRAS, 377, 1419
Wilman D. J., Pierini D., Tyler K., McGee S. L., Oemler Jr. A., Morris S. L., Balogh M. L., Bower R. G., Mulchaey J. S., 2008, ApJ, 680, 1009
Zheng X. Z., Bell E. F., Papovich C., Wolf C., Meisenheimer K., Rix H.-W., Rieke G. H., Somerville R., 2007, ApJ, 661, L41